

# Modeling and Numerical Analysis for Silicon-on-Insulator Rib Waveguide Corners

DeGui Sun, Xiaoqi Li, Dongxia Wong, Yuan Hu, Fangliang Luo, and Trevor J. Hall

**Abstract**—Silicon-on-insulator (SOI) waveguide designs have shown merit in highly integrated photonic devices and the associated manufacturing technique has achieved an acceptable level of maturity in the microphotonic industry. Thus, the sharp bending of SOI waveguides and/or deflection of light between SOI waveguides are the considerable interest for practical integrated SOI components. In this paper, a theoretical model is proposed for studying a variety of SOI rib waveguide corner mirror structures. Using the model, the precise positioning of the reflector is first studied, then the minimum acceptable reflector length and width are analyzed, and finally an effective reflecting interface (ERI) is found and determined by considering Goos-Hanchen effect. After being optimized with respect to the parameters: dimension (the length and width), position, surface roughness and tilt angle of mirror plane, and material refractive index of reflector, and their relations, the transfer efficiency of the corner mirror can achieve over 96% and 92% at the mirror-plane tilt-angles of respective 0° and 1° over a wide range of the corner angles of 80-120° even accounting for the 100-Å surface roughness of reflector is considered. The results of the model are validated via a full simulation using the commercial software tool: OptiFDTD.

**Index Terms**—Effective reflecting interface, optical transfer efficiency, silicon-on-insulator (SOI) rib waveguide, waveguide corner mirror.

Manuscript received May 08, 2008; revised October 17, 2008. First published June 19, 2009; current version published August 28, 2009. This work was cosponsored by the Ontario Centres for Excellences (CR-60017-08) of Canada, the R&D Foundation of the Changchun University of Science and Technology, and the Scientific Research Startup Foundation of the Chinese Academy of Sciences and Technology for Excellent Thesis for Doctor's Degree and the Gainer of Prior Award.

D. G. Sun is with the School of Information Technology and Engineering, University of Ottawa, Ottawa, ON, K1N 6N5, Canada, and also with the School of Optoelectrical Engineering, Changchun University of Science and Technology, Changchun JL 130022, China (e-mail: deguisun\_b@yahoo.com).

X. Li is with the State Key Laboratory of Applied Optics, Changchun Institute of Optics, Fine Mechanics and Physics, Chinese Academy of Sciences, Changchun, JL 130033, China, and also with the Graduate School of the Chinese Academy of Sciences, BJ 100039, China (e-mail: libaitian1015@163.com).

D. Wong is with D&T Photonics Inc., Ottawa, ON, K1T 4B3, Canada (e-mail: wongdongxia@163.com).

Y. Hu is with the School of Optoelectrical Engineering, Changchun University of Science and Technology, Changchun JL 130022, China (e-mail: huy@cust.edu.cn).

F. Luo is with the School of Information Technology and Engineering, University of Ottawa, Ottawa, ON, K1N 6N5, Canada and also with the Hefei Energy College of Vocation and Technology, Tangshan, Hebei 063004, China (e-mail: luofangliang@sina.com).

T. J. Hall is with the School of Information Technology and Engineering, University of Ottawa, Ottawa, ON, K1N 6N5, Canada (e-mail: thall@site.uottawa.ca).

Color versions of one or more of the figures in this paper are available online at <http://ieeexplore.ieee.org>.

Digital Object Identifier 10.1109/JLT.2009.2025609

## I. INTRODUCTION

AS THE developments and applications of optical communication and information transmission technology are quickly extending and microelectronic and semiconductor manufacturing technologies are becoming more mature, microphotonic has been forming a promising new branch of communication and information technology that complements microelectronics [1]. As a result, silicon-on-insulator (SOI) waveguides, technologies, and devices have been extensively studied in the past decade as a potential planar lightwave circuit (PLC) platform. In particular, the compatibility of the SOI-PLC technology with complementary metal oxide semiconductor (CMOS) technologies makes it possible to manufacture SOI-based photonic device products with commercially acceptable costs, and further form the hybrid integration of microphotonic and microelectronics on a single chip [1]–[3]. Many passive and active PLC components based on SOI waveguides, including Fabry–Perot microcavity- and microring-based components, switches, modulators, lasers, photo-detectors, and wavelength division multiplexing (WDM) devices (AWG), have been reported [3]–[8]. Furthermore, the inherent capabilities of and advances in SOI-PLC technology are encouraging intensive research on the hybrid integration of active and passive components on one chip [7]–[9].

Thereby, one may expect advances in microphotonic circuits similar to the advances made in microelectronics, including compact layout design, no-bending-loss-turning, multiple logic/processing functions and mature state of the art in manufacturing. So the development of photonic wires and logic units/technology is a prerequisite to the development of photonic processing chips or systems [9]–[11]. It is feasible to create photonic wires in SOI technology since the high refractive index contrast of SOI waveguides between Si layer and SiO<sub>2</sub> layer, an SOI waveguide, satisfying the single-mode (SM) transmission condition, confines light to subwavelength cross-sections. Such small dimensions however create difficulties in fabrication and coupling losses at interfaces between waveguides and fibers and active and passive devices on one chip [12], [13]. In this case, the rib waveguides are attracting attention because single-mode transmission can be realized at larger scales [13]–[15]. However, the minimum tolerable radius curvature of a conventional rib waveguide bend is quite large because of the lower optical confinement associated with the relatively small effective refractive index contrast of SOI waveguides in the lateral direction. To increase the integration density of PLC components on a single SOI chip, low-loss compact SOI waveguide bend and/or corner structures are essential. There have been a few reports of such waveguide

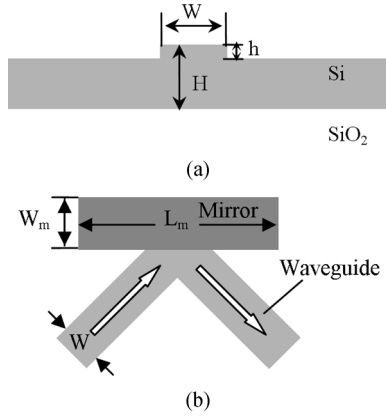


Fig. 1. (a) Cross-section of SOI waveguide structure and (b) SOI rib waveguide corner mirror geometry.

corner-mirror structures based on total internal reflection (TIR) including some earlier theoretical analyses [15]–[18]. In particular, [16] demonstrated the efficiency of corner mirrors in experiments with three typical substructures and effective manufacturing. However, no widely applicable theoretical model and systematic discussion have been reported so far on the design and optimization of the reflector for waveguide corners. Before the SOI rib waveguides were widely studied for highly integrated photonic devices, the simple corner mirror structures of rectangular waveguides were analyzed, but these works only considered the separate influences of limited physical factors [19], [20].

As we know, there is a set of equations to express both the electric and magnetic fields for a normal rectangular waveguide with Marcatili or Kumar’s analysis method, and for a rib waveguide an effective index method (EIM) was proposed and successfully deployed to transfer a rib waveguide into an equivalent rectangular waveguide [21], [22]. In this paper, a theoretical model for discussing the structure of a variety of SOI rib waveguide corner mirrors is proposed by taking into account both the EIM and the combined effect of the most significant physical factors. With the model, the impact of the accurate position, dimension (length and width), surface roughness and tilt angle of mirror plane, and material refractive index of reflector on the transfer efficiency of corner mirrors are studied and analyzed and then a theory of effective reflecting interface (ERI) is created.

## II. ANALYSIS OF THE REFLECTOR

The currently existing theoretical approaches for studying the waveguide corner-mirrors are all based on the optical TIR principle, but these approaches do not consider the confinement of light by the media and assume that the deflection of the light occurs at the geometric surface of the reflector according to TIR principle. In fact, the lightwave propagation in a waveguide structure with a reflector is strongly influenced by waveguide parameters because it is the confined mode(s) of a guided light wave in a waveguide channel rather than a plane wave of infinite extent. A cross-sectional view of the SOI rib waveguide studied in this work and the traditional geometry of rib waveguide corner are schematically shown in Fig. 1(a) and (b),

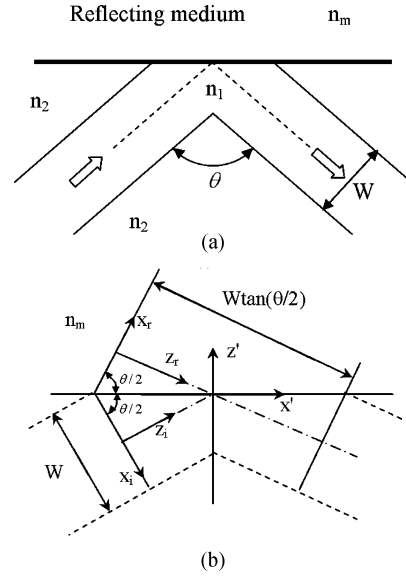


Fig. 2. (a) Equivalent slab waveguide configuration of the rib waveguide corner and (b) three coordinate systems for describing the incident and reflected waves.

respectively, where  $L_m$  and  $W_m$  are the length and width of reflector, respectively,  $W$  and  $h$  are the width and height of the SOI rib, respectively, and  $H$  is the total thickness of silicon layer of SOI waveguide structure. In order to obtain a more accurate physical model for the transfer efficiency of the corner mirror structure, we analyze the transmission property of the waveguide corner mirrors from the fundamental optical guided-mode principle.

### A. Position of the Reflector

In this section, the primary rib model is first transformed to an equivalent slab model by use of the EIM as shown in Fig. 2(a), which is composed of two regions—the upper region of reflecting medium and the lower region of waveguides, described using the coordinates system depicted in Fig. 2(b).

In this SOI rib waveguide system, the core and cladding layers of waveguides have the refractive indices  $n_1$  and  $n_2$ , respectively, and the reflecting medium has a refractive index  $n_m$ . As depicted in Fig. 2(a), the corner turning angle is  $\theta$ , the effective width of the equivalent slab waveguide core is  $W_{\text{eff}}$ , and the reflecting surface is located at the intersection point of the two waveguide axes [17], [18]. Here the discussion is limited to the incidence of the fundamental mode of weak confinement waveguides. In order to describe the incident and reflected waves, we transfer the rib waveguide shown in Fig. 1(a) to the equivalent rectangular waveguide with the EIM and exploit three different coordinate systems in Fig. 2(b): the normal coordinates  $(x, y, z)$ , the incident-wave coordinates  $(x_i, y_i, z_i)$ , and the reflected-wave coordinates  $(x_r, y_r, z_r)$ . The reflected-wave coordinates  $(x_r, y_r, z_r)$  are actually the image of incident-wave coordinates  $(x_i, y_i, z_i)$  with respect to the interface (the reflecting surface). In the rectangular Cartesian coordinates, here if  $E(x, y)$  is any electric field component, the separable solution of  $E(x, y) = E(x)E(y)$  is assumed by suppressing the time- and  $z$ -dependencies [22]. Thus at the

input plane, can be transformed to the spectral amplitudes as [18], [19]

$$\tilde{E}(k_x) = \int_{-\infty}^{\infty} E_i(x_i) \exp(jk_x x_i) dx_i \quad (1a)$$

$$\tilde{E}(k_y) = \int_{-\infty}^{\infty} E_i(y_i) \exp(jk_y y_i) dy_i \quad (1b)$$

where  $k_x$  and  $k_y$  are the propagation constants at the  $x$ - and  $y$ -directions, respectively. Similarly at the output plane,  $E_r(x_r)E_r(y_r)$  is given by

$$E_r(x_r) = \frac{1}{2\pi} \int_{-\infty}^{\infty} \tilde{E}(k_x) R(k_x) \times \exp \left[ -j \left( k_x x_r + W k_z \tan \frac{\theta}{2} \right) \right] dk_x \quad (2a)$$

$$E_r(y_r) = \frac{1}{2\pi} \int_{-\infty}^{\infty} \tilde{E}(k_y) R(k_y) \times \exp[-j(k_y y_r)] dk_y \quad (2b)$$

where  $k_z$  is the propagation constant at the  $z_i$ -direction and

$$k_x^2 + k_y^2 + k_z^2 = n_{\text{eff}}^2 k_0^2. \quad (3)$$

$R(k_x)$  and  $R(k_y)$  are the  $x$ - and  $y$ -components of the Fresnel reflection coefficient at the interface given by

$$R(k_x) = \frac{(k_{1x} - \eta k_{2x})}{(k_{1x} + \eta k_{2x})} \quad (4a)$$

$$R(k_y) = \frac{(k_{1y} - \eta k_{2y})}{(k_{1y} + \eta k_{2y})} \quad (4b)$$

where  $k_1$  and  $k_2$  are propagation constants in the  $z$ -direction in the lower and upper media, respectively, and can be expressed as two components in the  $x$  and  $y$ -directions as

$$k_{1x} = -k_x \sin \frac{\theta}{2} + k_z \cos \frac{\theta}{2} \quad (5a)$$

$$k_{1y} = k_0 \quad (5b)$$

$$k_{2x} = \left[ (n_m k_0)^2 - \left( k_x \cos \frac{\theta}{2} + k_z \sin \frac{\theta}{2} \right)^2 \right]^{1/2} \quad (6a)$$

$$k_{2y} = n_m k_0. \quad (6b)$$

The parameter  $\eta$  is defined as 1 for the transverse electric (TE)-mode and  $(n_{\text{eff}}/n_m)^2$  for the transverse magnetic (TM)-mode.

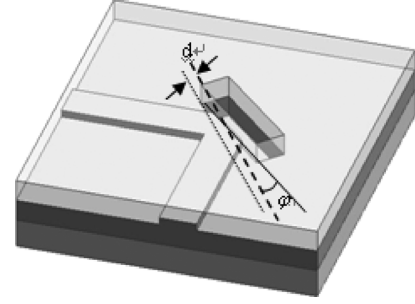


Fig. 3. SOI rib waveguide corner geometry. The reflector with a shift of  $d$ .

Then, if  $\sigma$  is the roughness of mirror plane, the transfer efficiency is determined by the overlap integral multiplied by an exponential function of  $\sigma$  as [19]

$$\tau = \left| \frac{\int E_r(x_r, y_r) E_o^*(x_r, y_r) dx_r dy_r}{\int E_o^2(x_r, y_r) dx_r dy_r} \right|^2 \cdot F_\sigma \quad (7)$$

where  $F_\sigma = \exp[-(2k_0 n_m \sigma \cos(\theta/2))]$  is the surface-roughness-induced light decay coefficient and  $E_0(x_r, y_r)$  is the transverse electric field of the fundamental mode in the output waveguide.

Goos and Hanchen's research showed that when a light wave strikes on a TIR interface, the effective reflecting interface is displaced from the geometric interface [23], [24]. This phenomenon of reflecting surface shift is referred to as Goos–Hanchen (GH) effect and the displaced distance is called the GH shift. To take the GH effect into the theoretical model, we set the reflector a tiny distance  $d$  along the  $z$  axis, where, as shown in Fig. 3,  $\varphi$  is the tilt angle of the mirror plane with respect to the vertical direction.

Thus, apart from the surface roughness  $\sigma$  of the mirror plane, the GH shift  $d$ , the tilt angle  $\varphi$  of the mirror plane, the corner angle  $\theta$ , and the refractive index  $n_m$  of reflector material can have a combined impact upon the optical power transfer efficiency  $\tau$  of the corner mirror system. After taking both  $d$  and  $\varphi$  into account, (2) should be changed to the new form as given in (8a) and (8b), shown at the bottom of the page, where  $R(k_x)$  and  $R(k_y)$  are still defined by (4a) and (4b), respectively, but the definitions of  $k_x$  and  $k_y$  are changed to

$$k_x = -k_{xi} \sin \left( \frac{\theta}{2} - \varphi \right) + k_{zi} \cos \left( \frac{\theta}{2} - \varphi \right) \quad (9a)$$

$$k_y = k_0 \cos \varphi \quad (9b)$$

$$E_r(x_r) = \frac{1}{2\pi} \int_{-\infty}^{\infty} \left( \cos 2\varphi + \frac{k_x}{k_z} \sin 2\varphi \right) \tilde{E}(k_x) R(k_x) \times \exp \left\{ -jk_x \left[ (\cos 2\varphi - \sin 2\varphi) x_r - 2d \sin \frac{\theta + 2\varphi}{2} \right] - jW k_z \tan \frac{\theta + 2\varphi}{2} \right\} dk_x \quad (8a)$$

$$E_r(y_r) = \frac{1}{2\pi} \int_{-\infty}^{\infty} \tilde{E}(k_y) R(k_y) \times \exp[-jk_y y_r \tan(90 - \varphi)] dk_y \quad (8b)$$

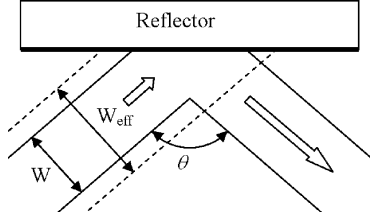


Fig. 4. Effective width and contact width calculation model of mode field.

$$k_z = k_{xi} \cos\left(\frac{\theta}{2} - \varphi\right) + k_{zi} \sin\left(\frac{\theta}{2} - \varphi\right). \quad (9c)$$

Note from (8a) and (8b) that in both  $E_r(x_r)$  and  $E_r(y_r)$ ,  $\varphi$  and  $\theta/2$  have the same amount contribution to the reflected wave, but  $\varphi$  has the negative effect, so it must be controlled at a very small value.

Further, the GH shift of this corner mirror is derived as

$$d = \frac{1}{k_0 \left[ n_1^2 \sin^2\left(\frac{\theta}{2} + \varphi\right) - n_m^2 \right]^{1/2}} = \frac{1}{\alpha_s} \quad \text{TE-Mode} \quad (10a)$$

$$d = \frac{n_m^2}{n_1^2 \sin^2\left(\frac{\theta}{2} + \varphi\right) - n_m^2 \cos^2\left(\frac{\theta}{2} + \varphi\right)} \cdot \frac{1}{\alpha_s} \quad \text{TM-Mode} \quad (10b)$$

where  $\alpha_s$  is the decay constant of the reflecting interface. Note from (8b) that the GH shift  $d$  has no impact upon the  $y$ -direction electric field of the output optical beam  $\tilde{E}_r(y_r)$ .

### B. Reflector Length

To realize the highest transfer efficiency with the reflector, a sufficient reflector length  $L_m$  is required to cover the whole signal area in the rib waveguide, so the modal field in a single-mode SOI rib waveguide should be first calculated. Then, as shown in Fig. 4, the effective width of the modal field is defined by

$$W_{\text{eff}} = W + \frac{2}{\alpha_w} \quad (11)$$

where

$$\alpha_w = k_0 \left( n_1^2 \sin^2 \frac{\pi}{2} - n_2^2 \right)^{1/2}. \quad (12)$$

$\alpha_w$  is the transverse decay constant. Then, the minimum length  $L_m$  of the reflector is given by

$$L_m = \frac{W_{\text{eff}}}{\tan \frac{\pi - \theta}{2}} + d. \quad (13)$$

Equation (13) indicates the inherent relation between the GH shift and the length of reflector, and this relation is also influenced by the effective width of channel waveguide. Namely, a rib waveguide can be transformed into an equivalent channel waveguide structure with an effective width and further determines the position and length of the reflector.

### C. Reflector Width

With the defined length, the reflector can cover almost all mode-field in one dimension, but the transfer efficiency is not

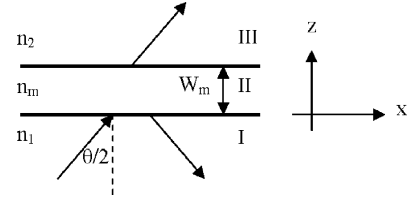


Fig. 5. Calculation modal for reflector width.

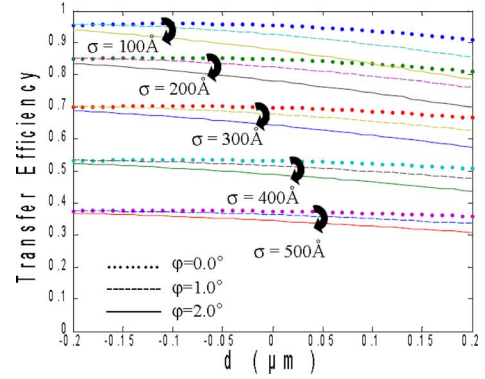


Fig. 6. Transfer efficiency of SOI waveguide corner mirror versus GH shift  $d$  at  $\lambda = 1.55 \mu\text{m}$  with three values of  $\varphi$  (dotted line:  $0^\circ$ , dashed line:  $1^\circ$ , and solid line:  $2^\circ$ ), where  $n_m = 1.0$ ,  $L_m = 8.0 \mu\text{m}$ ,  $W_m = 2.0 \mu\text{m}$ , and  $\theta = 90^\circ$ .

still ensured. So an optimal reflector width is necessary to reflect optical signal adequately. The geometric model for calculating the minimum reflector width  $W_m$  is shown in Fig. 5, where area I is waveguide having refractive index  $n_1$ , area II is reflector having refractive index  $n_m$ , and area III is cladding having refractive index  $n_2$ . Then, we have the solutions of the electric fields of optical signal as (14a)–(14c) in regions I, II, and III, respectively

$$E_I(z) = \exp(ik_0z) + R \exp(-ik_0z) \quad (14a)$$

$$E_{II}(z) = A \exp(-\chi z) + B \exp(\chi z) \quad (14b)$$

$$E_{III}(z) = C \exp(ik_0(z - W_m)) \quad (14c)$$

where  $k_0 = 2\pi/\lambda$ ,  $\chi = \sqrt{k_1^2 \sin^2(\theta/2) - k_2^2}$ ,  $k_1 = k_0 n_1$ ,  $k_2 = k_0 n_2$ , and  $\lambda$  is the wavelength in vacuum, and  $A$ ,  $B$ , and  $C$  are the normalized constants of optical signals. Further, by considering the boundary conditions, the interface reflection coefficient  $R$  between the reflector and the waveguide can be calculated as

$$R = -\frac{\chi + ik_0}{\chi - ik_0} \frac{1 - \exp(-2\chi W_m)}{1 - \exp(-2\chi W_m) r^2}. \quad (15)$$

Note that the reflector width  $W_m$  is determined by both the structure and material of both waveguide and reflector.

## III. NUMERICAL CALCULATIONS

With the systematic theoretical model defined by (1)–(15), we can calculate the dependence of reflector dimensions (length and width) on several important parameters such as the GH shift, corner angle, and material refractive index of reflector. All numerical calculations here are based on the free-space wavelength  $\lambda = 1.55 \mu\text{m}$ , the refractive index of core  $n_1 = 3.45$ ,

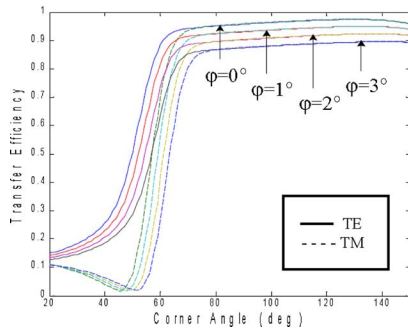


Fig. 7. Transfer efficiency of SOI waveguide corner mirror versus corner angle  $\theta$  at  $\lambda = 1.55 \mu\text{m}$ , where  $n_m = 1.0$ ,  $\sigma = 100 \text{ \AA}$  and  $d = -0.07 \mu\text{m}$ .

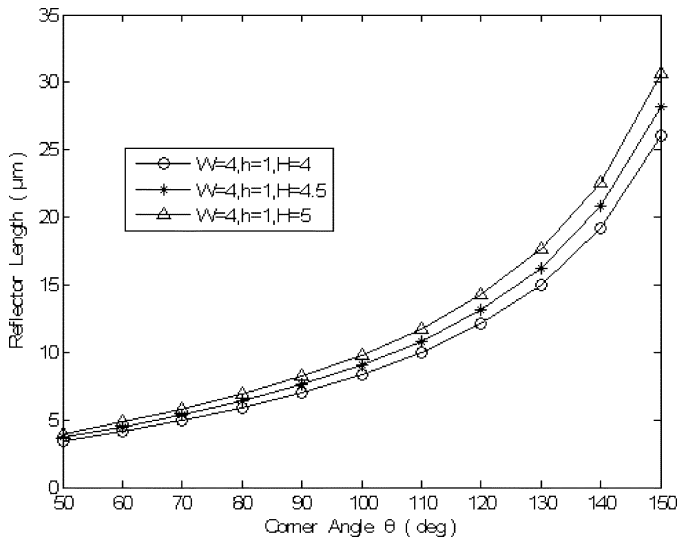


Fig. 8. Relation between reflector length  $L_m$  and corner angle  $\theta$ .

TABLE I  
RIB WAVEGUIDE CONFIGURATIONS AND CORRESPONDING REFRACTIVE INDICES (RI) OF THEIR EQUIVALENT SLAB WAVEGUIDES

Configuration ( $\mu\text{m}$ )	RI of core	RI of cladding	RI difference
$W=4, h=1, H=4.0$ ( $h/H=0.25$ )	3.4446	3.4405	0.12%
$W=4, h=1, H=4.5$ ( $h/H=0.22$ )	3.4458	3.4430	0.08%
$W=4, h=1, H=5.0$ ( $h/H=0.20$ )	3.4466	3.4446	0.06%

and the refractive index of cladding  $n_2 = 1.45$ , the width of the rib  $W = 4 \mu\text{m}$ , the height of the rib  $h = 1 \mu\text{m}$ , and the total thickness of the silicon layer  $H = 4 \mu\text{m}$ .

By selecting the reflecting medium of air ( $n_m = 1.0$ ),  $L_m \times W_m = 8 \mu\text{m} \times 2 \mu\text{m}$ , and with (8) and (9), first we calculated the transfer efficiency of a  $90^\circ$  corner architecture versus GH shift  $d$  with respect to five values of surface roughness  $\sigma$  of reflector and three values ( $0^\circ$ ,  $1^\circ$ , and  $2^\circ$ ) of tilt angle  $\varphi$  of mirror plane as shown in Fig. 6. Note that the optical transfer efficiency of the corner mirror structure has a maximal value of more than 96% at a negative value of GH shift  $d = -(0.07 \sim 0.20) \mu\text{m}$  when the reflecting surface roughness is  $\sigma = 100 \text{ \AA}$ . Further note that at the negative value of  $d$ , not only is the highest transfer efficiency achieved, but the dependence of the transfer efficiency

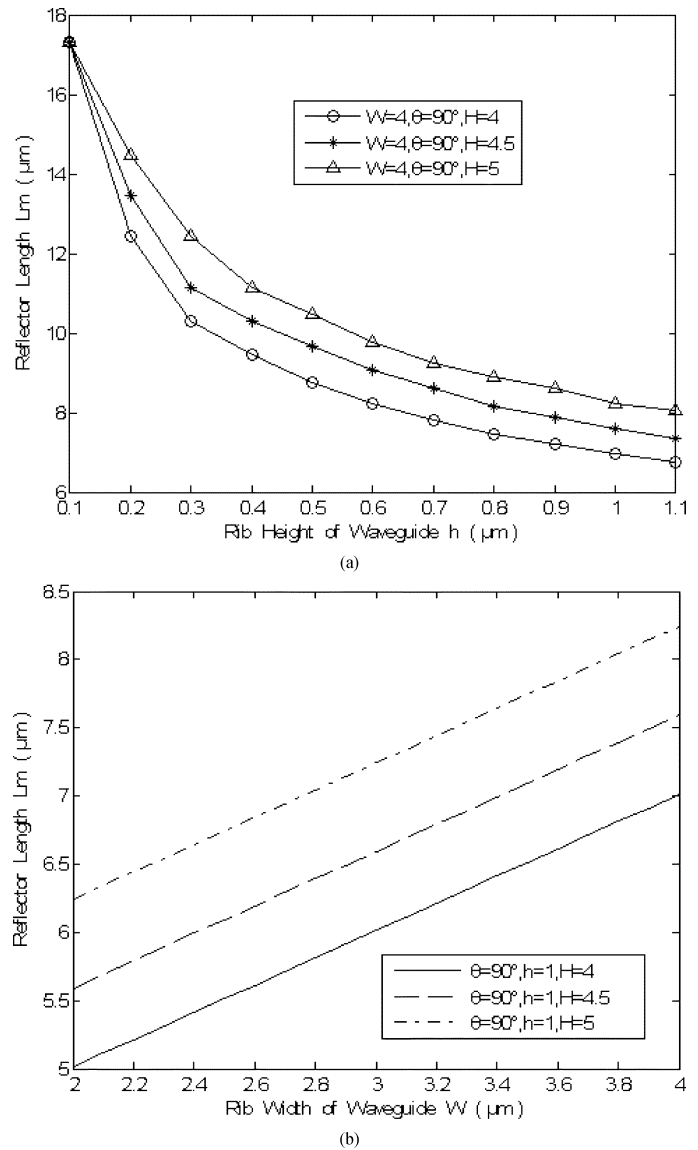


Fig. 9. Dependences of reflector length  $L_m$  on rib dimensions. (a) On rib height  $h$ . (b) On rib width  $W$ .

on the tilt angle of the reflector surface  $\varphi$  is very low and gradually reaches the lowest value as  $d$  approaches  $-0.20 \mu\text{m}$ . Thus, it is concluded that to optimize the transfer efficiency, the reflecting surface should be shifted a tiny distance to the inside of the corner, i.e., the GH shift value and at this shift value the effect of  $\varphi$  of less than  $2.0^\circ$  could be omitted. The GH shift is determined by several parameters of the device including the refractive index contrast of the reflector and waveguide materials, the corner angle and the waveguide structure. It turns out what reflects the optical beam is not the geometrical reflecting surface of the reflector, but an effective interface within the reflector. Thereby, the accurate calculation for the GH shift value is very conducive to the performance of some corner-mirror based device designs.

By setting the refractive index of reflector  $n_m = 1.0$ ,  $\sigma = 100 \text{ \AA}$  and GH shift  $d = -0.07 \mu\text{m}$ , further we calculated the transfer efficiency versus corner angle  $\theta$  with respect to four values of  $\varphi$  as shown in Fig. 7. Note that  $\varphi$  has a negative impact

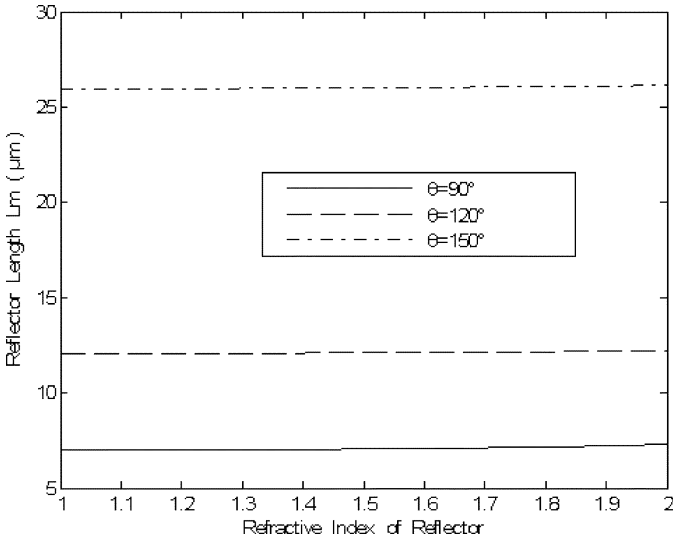


Fig. 10. Relation between length  $L_m$  and refractive index  $n_m$  of reflector.

on the transfer efficiency  $\tau$ , but if  $\varphi$  is not over  $2^\circ$   $\tau$  can achieve more than 90% and no longer has the polarization dependence when  $\theta$  is larger than  $80^\circ$ . Typically when  $\varphi = 0^\circ$  transfer efficiency  $\tau$  can achieve 96%, and even up to 98% at  $\theta = 120^\circ$ .

By setting the parameters—the refractive index of reflector  $n_m = 1.0$ —the relation between the reflector length  $L_m$  and the corner angle  $\theta$  (from  $50^\circ$  to  $150^\circ$ ) is obtained as shown in Fig. 8. Note that the reflector length  $L_m$  quickly increases with the corner angle  $\theta$  and also linearly increases with the total thicknesses  $H$  of the silicon layer. The reason is that a smaller value for the total thickness  $H$  of the silicon layer introduces a higher refractive index contrast of the equivalent channel waveguide and then produces a stronger confinement to the optical guided mode and vice versa. The parameter values of the equivalent channel waveguide with respect to the silicon layer  $H = 4, 4.5,$  and  $5 \mu\text{m}$  are listed in Table I. Fig. 8 and Table I can help select the reflector length to match the required corner angle.

It can be noticed from Table I that the waveguide is still a low refractive index contrast structure in the lateral direction, so it has weak confinement in this direction. That is why it can provide single-mode operation though having a relatively larger dimension ( $4 \mu\text{m}$ ) in the lateral direction. Further note from Fig. 8 that the required reflector length  $L_m$  decreases with the ratio of  $h$  to  $H$  ( $h/H$ ). But, the increase of  $h/H$  is restricted by the condition of single-mode operation because a higher  $h/H$  value can induce a multimode operation in waveguides.

Based on (11)–(13), the reflector length  $L_m$  is mainly determined by the configuration of the waveguide corner-turning mirror, which is easy to notice from the numerical results shown in Fig. 8. However, based on (14)–(15), the reflector width  $W_m$  is affected by the corner angle  $\theta$  and the refractive indices of both the waveguide and reflector rather than the configuration of rib waveguide. Here the waveguide is Si with a constant refractive index, so just the corner angle  $\theta$  and the refractive index of the reflector  $n_m$  need to be considered as variables to optimize the transfer efficiency of corner mirrors.

With respect to the total thickness of the silicon layer  $H = 4, 4.5$  and  $5 \mu\text{m}$ , and by taking the rib width  $W = 4 \mu\text{m}$ , the refrac-

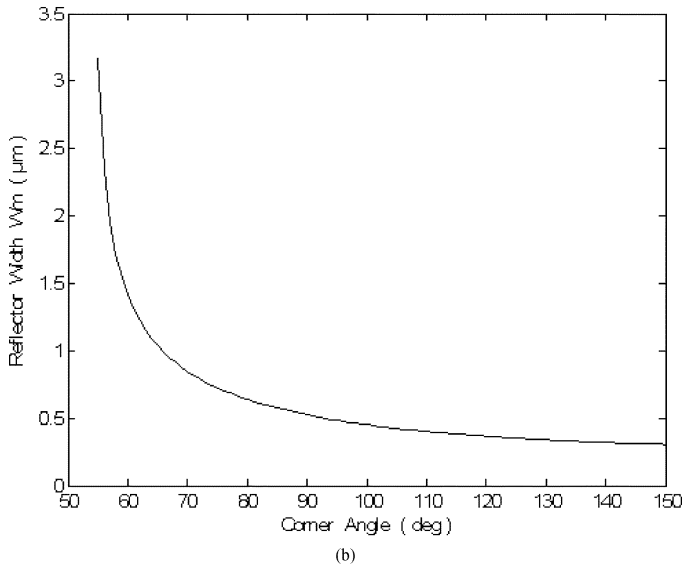
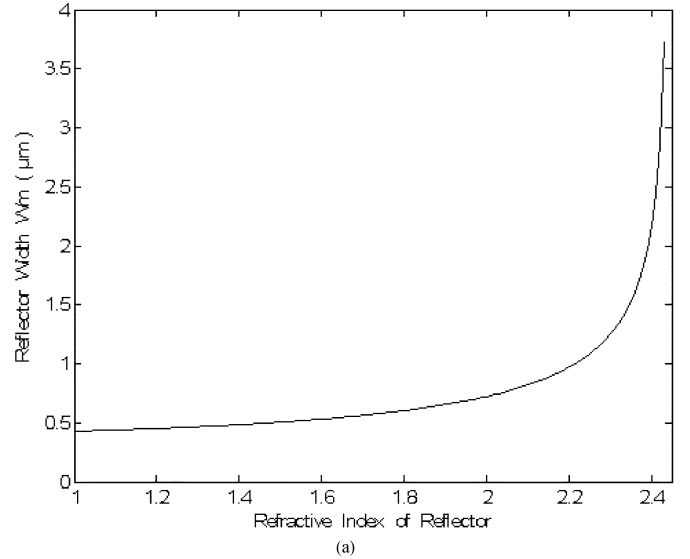


Fig. 11. (a) Relation between width  $W_m$  and refractive index of reflector for the corner angle of  $90^\circ$  and (b) the relation between reflector width  $W_m$  and corner angle for the reflector refractive index of  $n_m = 1.0$ .

tive index of reflector  $n_m = 1.0$ , and the corner angle  $\theta = 90^\circ$ , the dependences of the reflector length  $L_m$  on the rib height  $h$  and the rib width  $W$  are obtained as shown in Fig. 9(a) and (b), respectively. Note that  $L_m$  decreases with  $h$  and increases linearly with  $W$ . And like Fig. 8, Fig. 9 also indicates that the required reflector length decreases with the  $h/H$  value.

After analyzing the effect of the rib configuration on the optical transfer efficiency of reflector, the relation between the length  $L_m$  and the refractive index  $n_m$  of the reflector for the optimal optical transfer efficiencies with respect to the corner angle  $\theta = 90^\circ, 120^\circ,$  and  $150^\circ$  were calculated as shown in Fig. 10. Note that there is a linear relation between the reflector length and the refractive index of the reflector, and this relation almost keeps a constant irrespective of corner angle values; but more importantly, the reflector length quickly increases with corner angle.

Under one condition for the maximal transfer efficiencies ( $W = 4 \mu\text{m}, H = 4 \mu\text{m}, h = 1 \mu\text{m}, L_m = 8 \mu\text{m}, \sigma = 100 \text{ \AA}$ ,

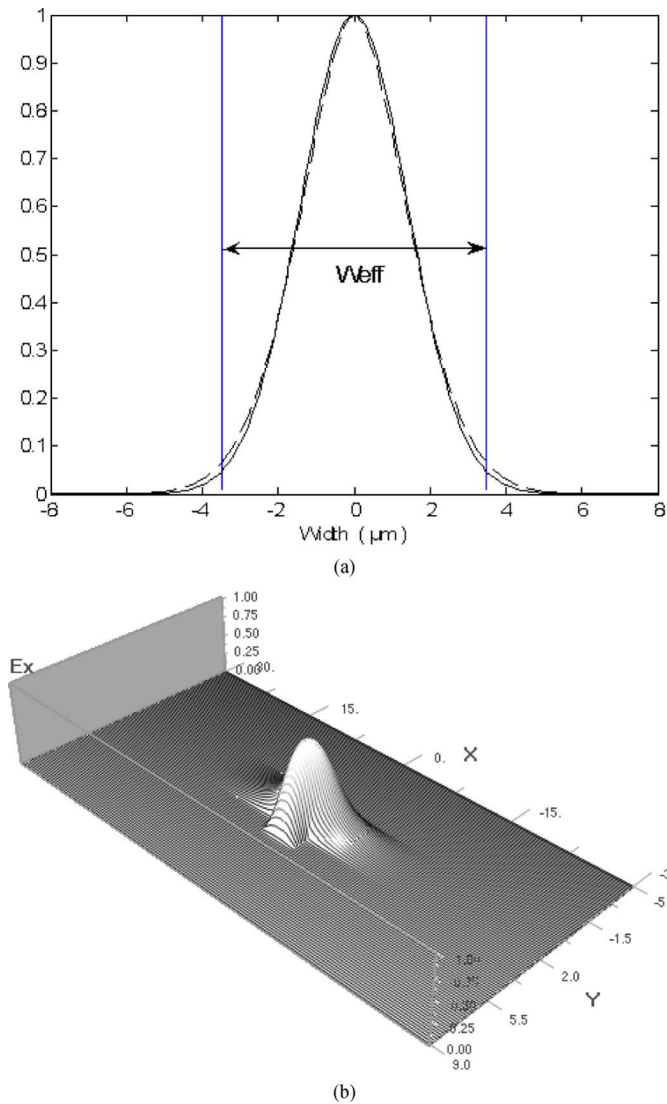


Fig. 12. BPM simulation of the mode distribution. (a) Accurate mode field of (dashed line) rib waveguide and (solid line) mode field precise optimized slab. (b) The simulation image of single mode distribution.

$\varphi = 0$ ), the relation between the reflector width  $W_m$  and the refractive index  $n_m$  of the reflector is obtained as shown in Fig. 11(a), and further the relation between the reflector width  $W_m$  and the corner angle  $\theta$  is also obtained as shown in Fig. 11(b). Note from Fig. 11(a) that the reflector width  $W_m$  increases with the refractive index  $n_m$ , and sharply increases when  $n_m$  approaches 2.43, the critical refractive index for total internal reflection. It can be noticed from Fig. 11(b) that the corner angle should be larger than  $70^\circ$ ; otherwise a too large reflector width would be required. This feature is consistent with the relation between the transfer efficiency and corner angle shown in Fig. 7.

In this section, the rib waveguide has been treated as an equivalent channel waveguide by the use of EIM, but there is still a difference between the fields within the two types of waveguides. With a given rib waveguide having the values of parameters  $W = 4 \mu\text{m}$ ,  $H = 4 \mu\text{m}$  and  $h = 1 \mu\text{m}$ , the field distribution of the guided-mode in the rib waveguide and its equivalent channel waveguide are simulated using Optiwave's BPM tool as

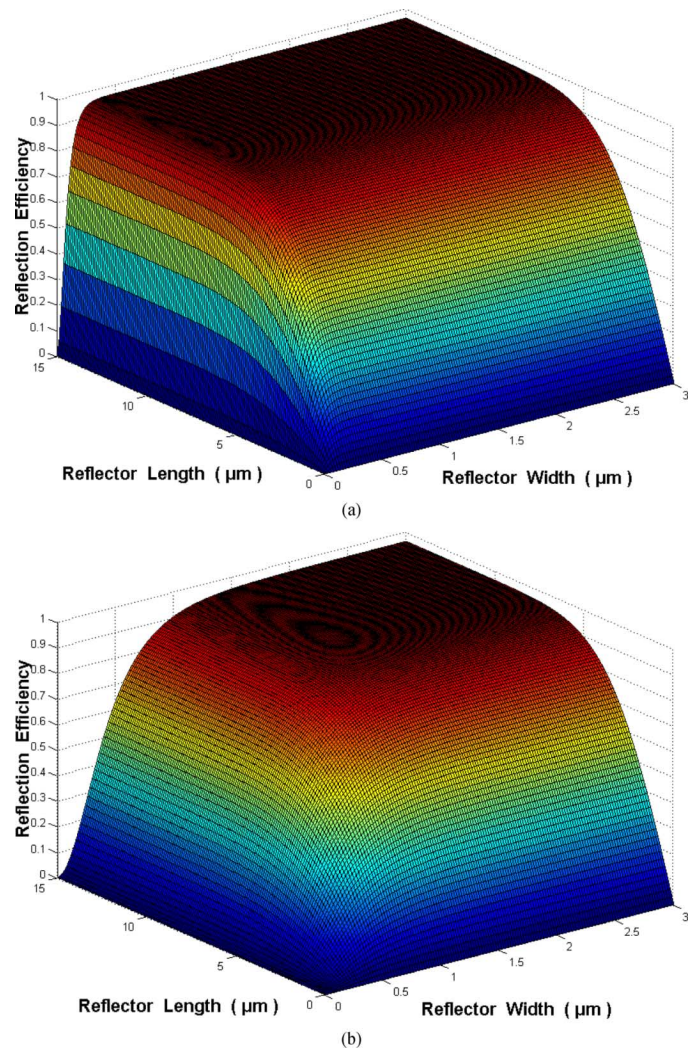


Fig. 13. Transfer efficiency versus reflector dimension (length  $L_m$  and width  $W_m$ ) when  $\theta = 90^\circ$ ,  $\varphi = 0^\circ$ , and  $\sigma = 100 \text{ \AA}$ , where (a)  $n_m = 1.0$  and  $d = -0.07 \mu\text{m}$  and (b)  $n_m = 2.4$  and  $d = -0.20 \mu\text{m}$ .

shown in Fig. 12(a), where the dashed line is for the rib waveguide and the solid line is for the equivalent slab waveguide, and the simulation image of single mode distribution in rib waveguide is shown in Fig. 12(b). In Fig. 12(a)  $W_{\text{eff}} = 6.94 \mu\text{m}$  is the effective width of the waveguide. Fig. 12 shows that the difference between the two fields is minimal and hence that the EIM used for the SOI rib waveguides herein is accurate enough.

From (11)–(15), the dependence of the optical transfer efficiency of the waveguide corner mirror structure on the reflector dimension ( $L_m$  and  $W_m$ ) and the corner angle  $\theta$  can be analyzed. Hence, at the corner angle  $\theta = 90^\circ$  and for two reflector materials ( $n_m = 1.0$  and  $n_m = 2.4$ ), the relationships between transfer efficiencies and reflector dimension are obtained as shown in Fig. 13(a) and (b), respectively. It is easy to notice from Fig. 13 that the transfer efficiency of reflector can achieve the maximal value of more than 96% at a small reflector size, and also the required minimal dimension of reflector for the maximal transfer efficiency increases with the refractive index value of reflector material. For instance, as shown in Fig. 13(a) and (b), the air reflector material ( $n_m = 1.0$ ) and the

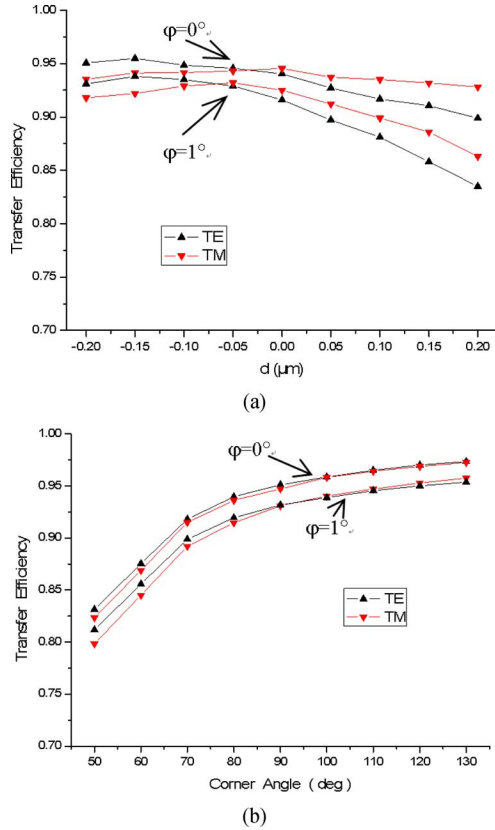


Fig. 14. Simulation results of transfer efficiency of waveguide corner mirror with commercial software: OptiFDTD with respect to  $\varphi = 0^\circ$  and  $\varphi = 1^\circ$ . (a) As a function of GH shift. (b) As a function of corner mirror angle, where  $n_m = 1.0$  and  $d = -0.07 \mu\text{m}$ .

other high-index reflector material (here it is taken as  $n_m = 2.4$ ) approximately require the reflector dimension ( $L_m \times W_m$ ) to be  $8 \mu\text{m} \times 1 \mu\text{m}$  and  $8 \mu\text{m} \times 2 \mu\text{m}$ , respectively.

In accordance with the simulation results obtained in Section III, the optimal structure of waveguide and corner mirror is chosen, which has the waveguide parameters  $W = 4 \mu\text{m}$ ,  $H = 4 \mu\text{m}$  and  $h = 1 \mu\text{m}$ , and the reflector parameters  $L_m = 8 \mu\text{m}$  and  $W_m = 2 \mu\text{m}$ , and then we verify its transfer efficiency with the Optiwave software tool: OptiFDTD. For the reflector material with the refractive index of  $n_m = 1.0$  and taking the reflecting surface roughness as  $100 \text{ \AA}$ , we obtain the transfer efficiencies versus the GH shift for the  $90^\circ$  corner mirror structure with respect to  $\varphi = 0^\circ$  and  $\varphi = 1^\circ$  as shown in Fig. 14(a). Note that around the GH shift of  $d = -0.07 \mu\text{m}$ , the transfer efficiency difference between TE and TM polarizations is smallest and the transfer efficiency itself is highest. Thus, after taking the GH shift of  $-0.07 \mu\text{m}$ , the transfer efficiency versus corner angle is further obtained as shown in Fig. 14(b). Note that the transfer efficiency increases with corner angle and at the  $90^\circ$  corner angle is over 95% and 92% corresponding to  $\varphi = 0^\circ$  and  $\varphi = 1^\circ$ , respectively, and the difference between TE and TM-polarizations can be almost ignored.

It turns out that the results obtained via commercial software tool not only agree well with each other between Fig. 14(a) and (b), but also strongly sustain the numerical

simulation results obtained with the aforementioned theoretical model depicted in Fig. 7.

#### IV. CONCLUSION

A large-size SOI rib waveguide corner mirror model, having the distinct advantage of being compact for optical integrated circuit application, has been designed. A whole theoretical model for the corner mirrors of SOI rib waveguides has been derived and discussed, and further the highly integrated SOI-based PLC devices has been proposed and analyzed. The relationships between the transfer efficiency and most of important parameters are simulated and the optimal structures of corner reflectors are obtained. For instance, both the waveguide structure and the corner mirror configuration, the material, accurate position, tilt angle of reflecting surface and configuration/dimension of the corner mirrors have all been calculated and discussed. The results of numerical calculations of the corner mirror have been analyzed. With the theoretical model, the corner mirror has achieved a transfer efficiency of over 96% for the ideal vertical mirror plane and 92% for the mirror plane having a tilt-angle of  $1^\circ$ . All the results demonstrated that the theoretical model is simple and efficient.

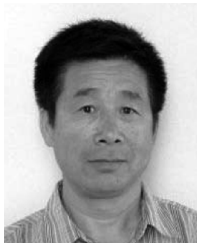
#### ACKNOWLEDGMENT

The authors would like to thank J. Liang, Y. Zhong, W. Li, and Z. Liang for their help to this work. T. Hall is grateful to the Canada Research Chairs program for his support.

#### REFERENCES

- [1] B. Jalali and S. Fathpour, "Silicon photonics," *J. Lightw. Technol.*, vol. 24, no. 12, pp. 4600–4615, Dec. 2006.
- [2] G. Roelkens, D. V. Thourhout, and R. Baets, "Silicon-on-insulator ultra-compact duplexer based on a diffractive grating structure," *Opt. Exp.*, vol. 15, pp. 10091–10096, 2007.
- [3] M. W. Pruessner, T. H. Stievater, M. S. Ferraro, and W. S. Rabinovich, "Thermo-optic tuning and switching in SOI waveguide Fabry–Perot microcavities," *Opt. Exp.*, vol. 15, pp. 7557–7563, 2007.
- [4] J. Niehusmann, A. Vorckel, P. H. Bolivar, T. Wahlbrink, and W. Henschel, "Ultrahigh-quality-factor silicon-on-insulator microring resonator," *Opt. Lett.*, vol. 29, pp. 2861–2863, 2006.
- [5] C. Z. Chao, A. H. Chen, E. K. Liu, and G. Z. Li, "Silicon-on-insulator asymmetric switches based on total internal reflection," *IEEE Photon. Technol. Lett.*, vol. 9, no. 8, pp. 1113–1115, Aug. 1997.
- [6] A. Liu, R. Jones, L. Liao, D. Samara-Rubio, D. Rubin, O. Cochen, R. Nicolaescu, and M. Paniccia, "A high-speed silicon optical modulator based on a metal-oxide-semiconductor capacitor," *Nature*, vol. 427, pp. 615–618, 2004.
- [7] T. Maruyama, T. Okumura, S. Sakamoto, K. Miura, Y. Nishimoto, and S. Arai, "GaInAsP/InP membrane BH-DFB lasers directly bonded on SOI substrate," *Opt. Exp.*, vol. 14, pp. 8184–8188, 2006.
- [8] K. Greene, "Intel Completes Photonics Trifecta," & "Silicon Lasers Get Up to Speed" [Online]. Available: [www.technologyreview.com](http://www.technologyreview.com)
- [9] B. Jalali, S. Yegnanarayanan, T. Yoon, T. Yoshimoto, I. Rendina, and F. Coppinger, "Advances in silicon-on-insulator optoelectronics," *IEEE J. Sel. Topics Quantum Electron.*, vol. 4, pp. 938–947, 1998.
- [10] Y. A. Vlasov and S. J. McNab, "Losses in single-mode silicon-on-insulator strip waveguides and bends," *Opt. Exp.*, vol. 12, pp. 1622–1631, 2004.
- [11] S. Ladenois, D. Pascal, L. Vivien, E. Cassan, S. Laval, R. Orobtcouk, M. Heitzmann, N. Bouzaida, and L. Mollard, "Low-loss submicrometer silicon-on-insulator rib waveguides and corner mirrors," *Opt. Lett.*, vol. 28, pp. 1150–1152, 2003.
- [12] R. A. Soref, J. Schmidtchen, and K. Peterman, "Large single-mode rib waveguides in GeSi-Si and Si-on-SiO<sub>2</sub>," *IEEE J. Quantum Electron.*, vol. 27, no. 8, pp. 1971–1974, Aug. 1991.

- [13] M. L. Tuma and G. Beheim, "Calculated coupling efficiency between an elliptical-core optical fiber and a silicon oxynitride rib waveguide," in *Proc. SPIE*, 1995, vol. 2383, pp. 199–210.
- [14] H. Chang, "Coupled-mode equations for dielectric waveguides based on projection and partition modal amplitudes," *IEEE J. Quantum Electron.*, vol. 23, no. 11, pp. 1929–1937, Nov. 1987.
- [15] R. U. Ahamd, F. Pizzuto, G. S. Camarda, R. L. Espinola, H. Rao, and R. M. Osgood, "Ultracompact corner-mirrors and T-branches in silicon-on-insulator," *IEEE Photon. Technol. Lett.*, vol. 14, no. 1, pp. 65–67, Jan. 2002.
- [16] Y. Qian, S. Kim, J. Song, and G. P. Nordin, "Compact and low loss silicon-on-insulator rib waveguide 90° bend," *Opt. Exp.*, vol. 14, pp. 6020–6028, 2006.
- [17] J. Ctyroky, H. Hokstra, L. Joannes, A. P. Leite, R. Pregla, and J. F. Vinchant, "Modelling of self-aligned total internal reflection waveguide mirrors: An inter-laboratory comparison," *Opt. Quantum Electron.*, vol. 27, pp. 935–942, 1995.
- [18] K. Ogusu, "Transmission characteristics of optical waveguide corners," *Opt. Commun.*, vol. 55, pp. 149–153, 1985.
- [19] A. Himeno, H. Terui, and M. Kobayashi, "Loss measurement and analysis of high-silica reflection bending optical waveguides," *J. Lightw. Technol.*, vol. 6, no. 1, pp. 41–46, Jan. 1988.
- [20] R. Orobtcouk, S. Laval, D. Pascal, and A. Koster, "Analysis of integrated optical waveguide mirrors," *J. Lightw. Technol.*, vol. 15, no. 5, pp. 815–820, May 1997.
- [21] K. Okamoto, *Fundamentals of Optical Waveguides*. San Diego, CA: Academic, 2000.
- [22] M. J. Adams, *An Introduction to Optical Waveguides*. New York: Wiley, 1981, ch. 6.
- [23] Y. Chung and N. Dagli, "Analysis of integrated optical corner reflectors using a finite-difference beam propagation method," *IEEE Photon. Technol. Lett.*, vol. 3, no. 2, pp. 150–152, Feb. 1991.
- [24] D. Dai, L. Liu, and S. He, "Analysis of integrated corner mirrors by using a wide-angle beam propagation method," *Opt. Commun.*, vol. 260, pp. 733–740, 2006.



**DeGui Sun** received the B.S. degree from the Harbin Institute of Technology, Harbin, China, in 1985, and the M.A.Sc. and Ph.D. degrees from the Changchun Institute of Optics and Fine Mechanics, Chinese Academy of Sciences, Changchun, China, in 1988 and 1993, respectively, all in electro-optic sciences and technologies.

From 1994 to 1998, he was a Postdoctoral Fellow in the Microelectronics Research Center, University of Texas at Austin. He then worked at Nu-Wave Photonics, Ottawa, ON, Canada, from March 1998 to December 2001. From January 2002 to July 2003, he worked as a Research Associate in the Quantum Photonics Laboratory, Northwestern University, Evanston IL. In 2003, his achievements were recognized by the Changchun Institute of Optics, Fine Mechanics and Physics, where he was appointed as a Research Professor and led and completed the 100-Talent-Plan Project of the Chinese Academy of Sciences until 2006. He also holds the title of Invited Professor of the Changchun University of Science and Technology (CUST) of China since 2004. He is currently a Research Scientist at the School of Information Technology and Engineering, University of Ottawa, ON, Canada. His interests include silicon-based integrated optics/photonics and technologies. He has 40 publications and has initiated eight patents related to integrated-optic devices.



**Xiaoqi Li** received the B.S. degree in optical communication from Jilin University, Jilin, China, in 2004, and the M.S. degree in optical engineering from the Changchun Institute of Optics, Fine Mechanics and Physics, Chinese Academy of Sciences (CIOMP), Jilin, China, in 2006. He is currently working toward the Ph.D. degree in CIOMP.

His major research interests include waveguide, optical communication, optical MEMS, optical devices, microoptical systems.

**Dongxia Wong**, photograph and biography not available at the time of publication.

**Yuan Hu**, photograph and biography not available at the time of publication.



**Fangliang Luo** received the B.S. degree from Hebei Normal University, Shijiazhuang, China, in 1982, and the M.E. and Ph.D. degrees from the University of Mining and Technology, Beijing, China, in 1993 and 2007, respectively.

Since 1982, he has been working in research on fiber optic sensors and communications. From October 2007 to December 2008, he worked as a Visiting Professor in the School of Information Technology and Engineering, University of Ottawa, Ottawa, ON, Canada. He is currently a Vice-President

of the Hebei Energy College of Vocation and Technology, Tangshan, China. He has participated in and managed some research projects, published more than ten papers, and obtained two patents. His major research interests include optical label switch, fiber optic sensors and communications, and voltage measuring and systems.



**Trevor J. Hall** studied general engineering, specializing in electrical sciences, at Christ's College, Cambridge University, Cambridge, U.K., from 1974–1977, where he received the B.A. degree in engineering in 1977 and the M.A. degree in engineering in 1981. His postgraduate research in fiber optics was conducted at University College London, London, U.K., where he received the Ph.D. degree in electronic engineering in 1980.

In 1979 he joined Cambridge Consultants Ltd as an Optical Physicist and then in 1980 joined Queen Elizabeth College London as a Lecturer in physics; moving to King's College London in 1984 following a merger. In 1993, he transferred to the Electronic Engineering Department, King's College London, to take up a position as Head of the Physical Electronics Research Group, and was subsequently promoted to Professor of optoelectronics in 1994. He joined the School of Information Technology and Engineering, University of Ottawa in 2002 as the Director of the Centre for Research in Photonic, University of Ottawa and as a Tier I Canada Research Chair in Photonic Network Technology. He has produced 326 publications (220 refereed) and initiated seven patents. The emphasis of his current research is on photonic networks and technology.

Dr. Hall is a member and Fellow of the Institute of Physics, a Chartered Scientist, an Engineer, and a Physicist. He is also a member and Fellow of the Institution of Engineering and Technology and has been a member of Optical Society of America since 2007.